

To be published in Astrophysical Journal

Implications of Quasar Black Hole Masses at High Redshifts

M. Dietrich ^{1,2} and F. Hamann ²,

dietrich@chara.gsu.edu

ABSTRACT

We investigated a sample of 15 luminous high-redshift quasars ($3.3 \lesssim z \lesssim 5.1$) to measure the mass of their super-massive black holes (SMBH) and compare, for the first time, results based on C IV, Mg II, and H β emission lines at high-redshifts. Assuming gravitationally bound orbits as dominant broad-line region gas motion, we determine black hole masses in the range of $M_{bh} \simeq 2 \times 10^8 M_\odot$ up to $M_{bh} \simeq 4 \times 10^{10} M_\odot$. While the black hole mass estimates based on C IV and H β agree well, Mg II typically indicates a factor of $\sim 5 \times$ lower SMBH masses. A flatter slope of the H β radius – luminosity relation, a possibly steeper slope of the Mg II radius – luminosity relation, and a slightly larger radius of the Mg II BLR than for H β could relax the discrepancy. In spite of these uncertainties, the C IV, Mg II, and H β emission lines consistently indicate super-massive black hole masses of several times $10^9 M_\odot$ at redshifts up to $z=5.1$. Assuming logarithmic growth by spherical accretion with a mass to energy conversion efficiency of $\epsilon = 0.1$ and an Eddington ratio L_{bol}/L_{edd} calculated for each quasar individually, we estimate black hole growth-times of the order of several ~ 100 Myr which are smaller than the age of the universe at the corresponding redshift. Assuming high-mass seed black holes ($M_{bh}^{seed} = 10^3$ to $10^5 M_\odot$) the SMBHs in the $z \simeq 3.5$ quasars began to grow at redshifts $z \gtrsim 4$, while for the quasars with $z \gtrsim 4.5$ they started at $z \simeq 6$ to 10. These estimated time scales for forming SMBHs at high redshifts, together with previous studies indicating high quasar metallicities, suggest that the main SMBH growth phase occurs roughly contemporaneously with a period of violent and extensive star formation in proto-galactic nuclei.

¹Department of Physics and Astronomy, Georgia State University, One Park Place South SE, Atlanta, GA 30303, USA.

²Department of Astronomy, University of Florida, 211 Bryant Space Science Center, Gainesville, FL 32611-2055, USA.

1. Introduction

During the last few years it has been established that almost all massive galaxies are hosting a super-massive black hole (SMBH) in their centers. It has been found that the SMHB mass is well correlated with the host galaxy's spheroidal component mass and with the bulge luminosity (e.g., Kormendy & Richstone 1995; Magorrian et al. 1998; McLure & Dunlop 2001). Furthermore, a remarkably close correlation of the SMBH mass and the stellar velocity dispersion, σ_* , is detected for active, as well as for non-active galaxies (Gebhardt et al. 2000; Graham et al. 2001; Merritt & Ferrarese 2001; McLure & Dunlop 2002; Tremaine et al. 2002). These results, together with indications that luminous quasars reside in massive early type galaxies (e.g., McLure et al. 1999; Kukula et al. 2001; Nolan et al. 2001; Percival et al. 2001; Dunlop et al. 2003), point to a closely related formation of massive spheroidal galaxies and the formation and growth of central SMBH. However, it is still under debate whether the black hole and the host galaxy formed simultaneously or whether one component formed before the other (e.g., Silk & Rees 1998; Cattaneo et al. 1999; Salucci et al. 1999; Kauffmann & Haehnelt 2000; Haiman & Loeb 2001; Menou et al. 2001; Archibald et al. 2002; Di Matteo et al. 2003).

It is of great importance to estimate SMBH masses at higher redshifts to investigate whether the relations of SMBH mass with fundamental parameters of their harboring galaxies that are found for active and non-active galaxies in the local universe are already established at early cosmic epochs. Recent studies of quasars at moderate (McLure & Jarvis 2002, $z \lesssim 1$) and high-redshifts (Shields et al. 2003, $z \lesssim 3$; Vestergaard 2004, $z \lesssim 6$) assume that the locally determined radius – luminosity relation can be applied up to redshifts of $z \simeq 6$. Particularly, black hole masses have been estimated for several high-redshift quasars, providing evidence that even at early cosmic times black holes with several times $10^9 M_\odot$ are already in place (Barth et al. 2003; Willott et al. 2003; Vestergaard 2004; Warner et al. 2004). The detection of quasars at redshifts $z \gtrsim 6$ (Fan et al. 2001) and black hole mass estimates well beyond $M_{bh} \simeq 10^{10} M_\odot$ (Bechtold et al. 2003; Netzer 2003) challenges black hole growth models to buildup SMBHs on time scales of several times ~ 100 Myr, because at $z \gtrsim 6$ the age of the universe is less than 0.9 Gyr. However, the high-redshift M_{bh} estimates are all based on the C IV $\lambda 1549$ emission line and the assumption of virialized gas motion. It is obviously important to use more than a single emission line to determine M_{bh} as a fundamental AGN parameter.

Much effort has been spent to derive methods to estimate the black hole mass, M_{bh} , based on reverberation experiments and assuming virial dominated motion of the broad line region (BLR) gas (e.g., Kaspi et al. 2000; Peterson & Wandel 1999, 2000; Wandel, Peterson, & Malkan 1999). This results in an empirically established radius-luminosity relation, $R_{BLR} \propto$

L^β with e.g. $\beta = 0.7$ (Kaspi et al. 2000). Since long-term variability studies are currently not feasible for quasars, alternative methods are suggested employing single epoch emission line profile width measurements to estimate M_{bh} (Vestergaard 2002). There is still some concern regarding this approach (e.g., Krolik 2001) and that the R-L relation might be flatter than $\beta = 0.7$ (e.g., Peterson et al. 2000; McLure & Jarvis 2002; Corbett et al. 2003; Netzer 2003; Vestergaard 2002, 2004 for a more detailed discussion). However, using emission line profiles of $H\beta$ and $CIV\lambda 1549$ to estimate the SMBH mass of quasars yields consistent results that are on average within $\sim 20\%$ (e.g., Vestergaard 2002; Warner et al. 2003). Recently, McLure & Jarvis (2002) suggested $Mg\,II\lambda 2798$ to measure black hole masses. Particularly for quasars at redshifts $z \gtrsim 4$, $Mg\,II$ is of great interest because $H\beta$ is shifted out of the K-band. As a low ionization line $Mg\,II$ can be used as a well suited replacement of $H\beta$ instead of using the high ionization line $CIV\lambda 1549$. In addition, independent methods based on the well established $M_{bh} \propto \sigma_*$ and $M_{bh} \propto M_{bulge}$ relations for active and non-active galaxies (Gebhardt et al. 2000; Ferrarese et al. 2001; Laor 2001; McLure & Dunlop 2001, 2002; Tremaine et al. 2002) result in consistent black hole mass estimates (see Barth 2003; Vestergaard 2004 for a more detailed discussion).

In the following we present the results of SMBH mass estimates for luminous quasars at redshifts $3.3 \lesssim z \lesssim 5.1$ that we observed in the near infrared to study the evolution of the $Fe\,II/Mg\,II$ emission line ratio (Dietrich et al. 2002a, 2003a). We analyzed the broad emission line profiles of $Mg\,II\lambda 2798$ and $H\beta$. For most of the quasars we also have observed or have access to the ultraviolet spectral range that contains the strong $CIV\lambda 1549$ emission line. Hence, we could use almost always at least two emission line profiles to determine M_{bh} and for the first time to compare the obtained SMBH masses.

In the following we assume $H_o = 65 \text{ km s}^{-1} \text{ Mpc}^{-1}$, $\Omega_M = 0.3$, $\Omega_\Lambda = 0.0$. Introducing $\Omega_\Lambda = 0.7$ (Netterfield et al. 2002) instead of $\Omega_\Lambda = 0.0$, the luminosities at the highest redshifts would be $\sim 10\%$ larger. Hence, a slight change in luminosity will only have a minor impact on the estimated black hole mass.

2. The High-Redshift Quasar Sample

We have observed a sample of 15 luminous high-redshift quasars with $z \simeq 3.3$ up to $z \simeq 5.1$ (Table 1). The spectra were obtained using infrared and optical spectrographs of the Cerro Tololo Inter-American Observatory at Chile (OSIRIS, 4 m), the ESO observatories at La Silla (SofI, 3.5 m) and Paranal (ISAAC, 8.2 m) at Chile, the Calar Alto Observatory (Twin, 3.5 m) at Spain, and the W.M. Keck Observatory (NIRSPEC, 10 m) at Hawai'i (for more details on the observations see Dietrich et al. 1999, 2002a, 2003a; Dietrich & Wilhelm-

Erkens 2000). In order to study the broad ultraviolet Fe II emission and the Mg II λ 2798 emission line ratio J, H, and K-band spectra were recorded. For the quasars with $z \simeq 3.5$ we observed in the K-band the rest frame optical wavelength range which covers H β and [O III] λ 4959, 5007. Furthermore, for 10 of the studied quasars we have ultraviolet spectra of the C IV λ 1549 emission line (Dietrich et al. 2002b).

3. Data Analysis

3.1. Emission Line Profile Measurements

For each of the high-redshift quasars we measured the emission line profile width of H β , Mg II λ 2798, and C IV λ 1549 if covered. To determine a reliable profile width it is necessary to identify and to remove potential contamination by additional emission features. Although the Mg II λ 2798 emission line doublet appears to be relatively isolated in quasar spectra, it is embedded in the superposition of many thousands of discrete ultraviolet Fe II emission lines that form broad emission blends (e.g., Wills, Netzer, & Wills 1985). The careful correction for ultraviolet Fe emission yields a more solid measurement of the Mg II profile width than assuming a linear pseudo-continuum beneath the Mg II emission line. The contamination of H β by optical Fe II emission is less severe (e.g., Boroson & Green 1992). C IV λ 1549 suffers only minor contamination of weak emission lines, like N IV] λ 1486 in the blue wing and from Fe II emission beneath the C IV line profile (e.g., Vestergaard & Wilkes 2001). To account for these emission line profile contaminations we analyzed the high redshift quasar spectra using a multi-component fit approach (Dietrich et al. 2002a, 2003a). Following Wills, Netzer, & Wills (1985) we used the following four components to reconstruct each quasar spectrum, (i) a power-law continuum ($F_\nu \sim \nu^\alpha$), (ii) Balmer continuum emission (Grandi 1982; Storey & Hummer 1995), (iii) Fe II emission templates for the ultraviolet and optical wavelength range (Vestergaard & Wilkes 2001; Boroson & Green 1992), and (iv) Gaussian profiles to account for individual broad emission lines, such as H β , Mg II, and C IV. The power-law continuum fit to the individual quasar spectra was iteratively determined taking into account the measured strength of the Fe II emission and Balmer continuum emission derived by the fitting process. The emission line profile widths, expressed as full width at half maximum (FWHM) which we measured for H β , Mg II, and C IV if are accessible, are given in Table 2, together with the spectral slope α of the power-law continuum. Since the spectral resolution of the infrared spectra is of the order of ~ 200 to 500 km s $^{-1}$ (Table 2), a correction of the measured profile width with respect to the instrumental resolution is not necessary.

3.2. Estimating Black Hole Masses

The empirically justified radius-luminosity relation, $R_{BLR} \propto L^\beta$ (e.g., $\beta = 0.7$, Kaspi et al. 2000) and the assumption of virial dominated motion of the broad line region (BLR) gas (Peterson & Wandel 1999; Onken & Peterson 2002) has led to equations which connect the black hole mass M_{bh} with observationally accessible parameters like luminosity and emission line profile width. We applied the equations given by Kaspi et al. (2000), McLure & Jarvis (2002), Vestergaard (2002), and Warner et al. (2003) to estimate the black hole mass for the high-redshift quasars we observed. The explicit form of the equations we employed, are presented in the appendix for $H\beta$, $Mg\text{II}\lambda 2798$, and $C\text{IV}\lambda 1549$.

It should be kept in mind that although $C\text{IV}\lambda 1549$ is a high-ionization emission line, in contrast to $H\beta$ and $Mg\text{II}\lambda 2798$ as typical low-ionization lines, there are good reasons to assume that the broad line $C\text{IV}$ emitting gas motion also is gravitationally dominated (Peterson & Wandel 2000). This assumption is based on variability response, the emission line profile shape, and the relation of the profile widths of $H\beta$ and $C\text{IV}\lambda 1459$ combined with variability time lags (Onken & Peterson 2002). Furthermore, it has been shown that using emission line profiles of $H\beta$ and of $C\text{IV}\lambda 1549$ to estimate the SMBH mass of quasars yields consistent results on average (e.g., Vestergaard 2002; Warner et al. 2003).

4. Results

4.1. Super Massive Black Hole Mass Estimates

We applied the equations (A1) to (A5) given in the appendix together with the emission line profile widths of $H\beta$, $Mg\text{II}$, and $C\text{IV}$ and the spectral index α of the continuum slope (Table 2), to calculate the mass of the SMBH for each of the high-redshift quasars. To estimate the uncertainty of the determined SMBH masses the errors of the emission line profile width measurements and of the continuum luminosity have been propagated. In Table 3 the resulting black hole masses for each emission line estimator are presented. In Figure 1 the black hole mass is displayed for each emission line as a function of redshift. The luminous quasars under study have black hole masses in the range of $M_{bh} \simeq 2 \times 10^8 M_\odot$ up to $M_{bh} \simeq 4 \times 10^{10} M_\odot$. The SMBH mass based on the $H\beta$ profile width are consistent within a factor of $\sim 1.9 \pm 0.1$, with lower mass estimates provide by the relation suggested by McLure & Jarvis (2002) compared to those of Kaspi et al. (2000). This difference is mainly caused by the different slopes of the applied $R - L$ relation. Assuming a slope of $\beta = 0.6$ instead of $\beta = 0.7$ will result in ~ 2 times lower M_{bh} estimates. Utilizing the $C\text{IV}$ emission line profile width, the resulting SMBH mass estimates, using equations A3 and A4 as given

in the appendix, are consistent within $\sim 15\%$, as expected since the same slope is assumed for the R – L relation (eqs. A3 and A4). The scatter of the two SMBH estimates based on C IV are due to the use of the individual spectral index α for each quasar that we determined instead of using a uniform continuum slope of $\alpha = -0.4$ for example. Furthermore, to use the continuum luminosity $L(1450 \text{ \AA})$ for each quasar an additional α -dependent factor is introduced. In spite of these modifications the resulting black hole mass estimates, using the C IV profile width, agree well with each other. Close inspection of Figure 3 obviously shows that the M_{bh} estimates based on Mg II are systematically lower than the ones based on H β and C IV $\lambda 1549$. On average the Mg II $\lambda 2798$ emission line profile indicates a $\sim 5 \times$ lower SMBH mass than the H β and C IV $\lambda 1549$ line profile. For each of the high-redshift quasars we calculated a mean SMBH mass based on H β , Mg II, and C IV if available (Table 3). Although the SMBH mass estimates based on Mg II are lower than those given by H β and C IV, we do not apply possible corrections (see Sect. 4.2).

4.2. Size of the MgII Emission Region

A basic assumption of the R–L relation involving the Mg II $\lambda 2798$ emission line is that the emission regions of Mg II and H β are nearly at the same distance from the central continuum source. While the comparison of the profile width of both emission lines indicate that $R_{BLR}(H\beta)$ is nearly identical with $R_{BLR}(\text{MgII})$ (McLure & Jarvis 2002), Corbett et al. (2003) find that Mg II has generally a broader profile than H β . In Figure 2 we compare the FWHM of the line profiles of Mg II and H β for the seven quasars at $z \simeq 3.5$. With the exception of Q 2050–359 and Q 0105–2634 (similar width) and Q 2348–4025 (larger Mg II profile than H β) the H β profile is generally slightly broader than the Mg II profile. The average ratio of the FWHM of the H β to Mg II $\lambda 2798$ line profile amounts to 1.2 ± 0.5 based on the seven $z \simeq 3.5$ quasars we studied.

The most direct measure of the BLR radius for Mg II is given by reverberation mapping experiments. So far, almost all monitoring campaigns dedicated to AGNs have been focused in the optical on the H β region and in the ultraviolet on the Ly α – C IV $\lambda 1549$ – C III] $\lambda 1909$ wavelength range. However, for NGC 5548 (Clavel et al. 1991; Peterson et al. 1991; Dietrich & Kollatschny 1995) and NGC 3783 (Reichert et al. 1994; Stirpe et al. 1994) Mg II $\lambda 2798$ and H β were measured. NGC 3783 showed only minor Mg II emission line flux variations during the seven month campaign in 1992. The derived emission line flux variation delays for Mg II and H β are of the same order of $\tau \simeq 6 - 8$ days (Reichert et al. 1994; Stirpe et al. 1994). In contrast, NGC 5548 underwent quite strong variations for H β and Mg II during the first year of its monitoring in 1989. Dietrich & Kollatschny (1995) used the NGC 5548

observations taken with IUE in the ultraviolet (Clavel et al. 1991) and from the ground-based monitoring campaign (Peterson et al. 1991) to estimate a typical radius of the Mg II $\lambda 2798$ and H β emission line regions. They determined time delays based on the centroid (τ_c), as well as on the peak (τ_p), of the interpolated cross-correlations function (ICCF). The time delays based on the ICCF centroid amount to $\tau_c(\text{H}\beta) = 19.7 \pm 2.4$ d and $\tau_c(\text{MgII}) = 46.5 \pm 2.3$ d, while the peak of the ICCF yield delays of $\tau_p(\text{H}\beta) = 19.5 \pm 2.4$ d and $\tau_p(\text{MgII}) = 39.5 \pm 3.3$ d (Dietrich & Kollatschny 1995). Assuming that these delays represent typical distances of the line emitting gas from the central variable continuum source, in the case of NGC 5548 the Mg II gas is located ~ 2 times more distant than the H β emitting region. In a very simplified model of gravitationally bound Keplerian orbits it can be expected that the typical velocity of Mg II is about $\sqrt{2}$ times narrower than for H β . However, this estimate of $R_{BLR}(\text{MgII})$ is based on only one Seyfert galaxy. Although this result is quite consistent with the ratio of the profile widths of H β to Mg II that we find for the high-redshift quasars (Figure 2 and Table 2), it is necessary to measure $R_{BLR}(\text{MgII})$ for more Seyfert galaxies and quasars. Since a larger distance of the Mg II BLR emitting region than for H β will introduce a factor of $b = R_{BLR}(\text{MgII})/R_{BLR}(\text{H}\beta)$, the estimated SMBH mass will be slightly underestimated assuming $R_{BLR}(\text{MgII}) \simeq R_{BLR}(\text{H}\beta)$.

4.3. Bolometric Luminosity and Eddington Ratio

To compare the SMBH mass with the bolometric luminosity, L_{bol} , and to determine the Eddington luminosity ratio, L_{bol}/L_{edd} , we calculated L_{bol} . To transform measured rest frame luminosities λL_λ into L_{bol} scaling factors are provided by e.g. Elvis et al. (1994) and Kaspi et al. (2000). Most recently, Vestergaard (2004) and Warner et al. (2004) present revised scaling factors for optical and ultraviolet continuum luminosities employing results of multi-frequency studies on the AGN spectral energy distributions from X-ray energies to the mid-infrared wavelength range. They found consistent scaling factors which are slightly smaller ($\sim 20\%$) than previously assumed. We used the relation $L_{bol} = 4.36 \times \lambda L_\lambda(1450\text{\AA})$ to calculate the bolometric luminosity (Warner et al. 2004) for each of the high-redshift quasars under study (Table 1). In Figure 3 we plot the average SMBH masses as a function of L_{bol} . At a given L_{bol} the determined M_{bh} of the high-redshift quasars cover a range of up to one order of magnitude in mass, similar to comparable studies for quasars at lower redshift (e.g., Woo & Urry 2003; Vestergaard 2004; Warner et al. 2004).

For a fully ionized pure hydrogen gas, i.e. $\mu_e = 1$, the Eddington luminosity is given as (Rees 1984; Peterson 1997)

$$L_{edd} = 1.26 \times 10^{38} \left(\frac{M_{bh}}{M_{\odot}} \right) \mu_e \text{ erg s}^{-1} \quad (1)$$

Assuming a more realistic gas chemical composition containing hydrogen, helium, and some heavier elements will result in an additional factor $\mu_e = 1.15$ accounting for the atomic weight per electron (Haiman & Loeb 2001). This will yield a 15% higher Eddington luminosity. In the following we will assume pure hydrogen gas because $\mu \neq 1$ has only minor impact on L_{edd} .

The Eddington ratio L_{bol}/L_{edd} is determined for each quasar individually. The mean black hole masses are used to calculate the Eddington luminosity, L_{edd} , for spherical accretion. Together with the bolometric luminosity, the Eddington ratio, L_{bol}/L_{edd} , is calculated (Table 3). The determined L_{bol}/L_{edd} covers a range of ~ 0.5 to ~ 7 which is in good agreement with results of studies of quasars sample that are dominated by low and intermediate redshift quasars (e.g., Woo & Urry 2003; Vestergaard 2004; Warner et al. 2004). Hence, there is no difference regarding the Eddington ratio L_{bol}/L_{edd} for quasars at high-redshifts compared to those at lower redshift.

5. Discussion

5.1. Comparison of M_{bh} based on H β , Mg II, and C IV

In Table 3 the SMBH mass estimates based on the three emission lines H β , Mg II $\lambda 2798$, and C IV $\lambda 1549$ are listed for comparison. Similar to previous studies there appears to be an approximate upper limit for M_{bh} at $\sim 10^{10} M_{\odot}$ (e.g., Corbett et al. 2003; Netzer 2003; Shields et al. 2003; Vestergaard 2004; Woo & Urry 2003; Warner et al. 2003). Only Q 0105-2634 yields an estimate of $M_{bh} = (4.1 \pm 1.2) \times 10^{10} M_{\odot}$ (eq. A1) and $(2.1 \pm 0.4) \times 10^{10} M_{\odot}$ (eq. A2), respectively, based on the H β emission line width. However, the H β emission profile of this particular quasar has a rather low signal-to-noise ratio. Furthermore, the estimate $M_{bh} = (4.1 \pm 1.2) \times 10^{10} M_{\odot}$ based on the R-L relation with a slope of $\beta = 0.7$. Assuming a flatter slope β of the R-L relation, as suggested by Peterson et al. (2000) and McLure & Jarvis (2002) the mass estimate is reduced by a factor of ~ 2 and in this case within the uncertainties in better agreement with an empirical upper limit of $M_{bh}^{max} \simeq 10^{10} M_{\odot}$ which also has been suggested by Umemura (2003) and Rocca-Volmerange et al. (2004) who studied early phases of galaxy formation and related black hole growth.

For two quasars at redshift $z \simeq 3.5$ we detected quite prominent [O III] $\lambda 4959, 5007$ emission. It has been suggested that the emission line profile width of [O III] $\lambda 4959, 5007$

can be used as a surrogate of the stellar velocity dispersion σ_* (Nelson 2000). Applying the relation that connects black hole mass with stellar velocity dispersion (Tremaine et al. 2002) the use of [O III] $\lambda 4959, 5007$ as a SMBH mass estimator has been investigated by Shields et al. (2003). Using the emission line profile width of [O III] $\lambda 5007$ the estimated the mass of the black holes amount to $1.4 \pm 0.3 \times 10^9 M_\odot$ (Q 0256-0000) and $1.5 \pm 0.3 \times 10^9 M_\odot$ (Q 0302-0019) which are consistent with the masses provided by C IV, Mg II, and H β (Table 3).

While the black hole mass estimates based on C IV $\lambda 1549$ and H β are quite consistent, the M_{bh} estimate provided by Mg II $\lambda 2798$ indicates lower masses (Table 3). Although R – L relations based on statistical results found for quasar samples introduce uncertainties of a factor of at least ~ 3 in the case of individual quasars (e.g., Vestergaard 2002) there are some additional possibilities which may cause lower M_{bh} estimates based on Mg II $\lambda 2798$.

First, the slope β of the $R \propto L^\beta$ relationship is still not well defined, varying between ~ 0.5 to 0.7 (e.g., Kaspi et al. 2000; Peterson et al. 2000; McLure & Jarvis 2002; Vestergaard 2002; Netzer 2003). A flatter slope in the R – L relation will result in less massive black holes. While in the original analysis by Kaspi et al. (2000) it is found that $\beta = 0.70 \pm 0.03$, there are indications that the slope is closer to $\beta \simeq 0.62 \pm 0.02$ (Peterson et al. 2000). McLure & Jarvis (2002) derived $\beta = (0.47 \pm 0.05)$ for the R – L relation using Mg II. They determined this flatter slope under the assumption that Mg II and H β originate at nearly the same BLR radius. Hence, they used H β reverberation results for Seyfert galaxies and quasars to analyze the correlation of $r_{BLR}(\text{Mg II})$ with the luminosity $\lambda L_\lambda(3000)$. However, assuming a slightly flatter slope of $\beta = 0.6$ instead of $\beta = 0.7$ will decrease the estimated black hole mass based on H β by a factor of ~ 2 . Using furthermore a slightly steeper slope for Mg II (e.g., $\beta = 0.6$ instead of $\beta = 0.47$) will provide on average $\sim 2.4 \pm 0.2$ times higher SMBH estimates. A second aspect as discussed in Sect. 4.2 is the size of the Mg II emitting region. If Mg II originates at slightly larger distances to the center of the continuum emission than H β , the estimated mass can be increased by an additional factor. Currently, we suppose that the different SMBH estimates provided by C IV and H β compared to those based on Mg II are predominantly caused by the different slopes of the R-L relations. Furthermore, it is still an open question whether the R-L relation can be extrapolated to quasar luminosities since the relation is derived for active galactic nuclei with $L_{bol} \lesssim 10^{46} \text{ erg s}^{-1}$ (e.g., Corbett et al. 2003). In the case of quasars this relation is extended to $\sim 10^2$ to $\sim 10^3$ times more luminous objects. Yet, in spite of the uncertainties regarding the use of the H β , Mg II, and C IV emission line profiles to determine the black hole mass, we emphasize that all three emission lines indicate consistently the presence of super-massive black holes with masses of $10^9 \lesssim M_{bh} \lesssim 10^{10} M_\odot$ at redshifts up to $z=5.1$.

5.2. Implications of Black Hole Growth Time Scales

The presence of SMBHs at high-redshifts and the close relation of quasar activity and galaxy formation provide valuable constraints on the epoch when these SMBHs had to start to grow in their forming host galaxies. The time span that is necessary to build-up a $\sim 10^9$ to $10^{10} M_\odot$ SMBH can be described by an e-folding time for the growth of a single seed black hole (e.g., Haiman & Loeb 2001). We use the following equation to estimate the e-folding time scale and hence the epoch when the seed black hole started to grow (Salucci et al. 1999)

$$M_{bh}(t_{obs}) = M_{bh}^{seed}(t_o) \exp\left(\frac{\eta\tau}{\epsilon t_E}\right) \quad (2)$$

with $\tau = t_{obs} - t_o$ as time elapsed from the initial time, t_o , to the observed time, t_{obs} , M_{bh}^{seed} as seed black hole mass, $\eta = L_{bol}/L_{edd}$ as Eddington ratio, ϵ as efficiency to convert mass to energy, and t_E as Eddington time scale, with $t_E = \sigma_T c / 4\pi G m_p = 3.92 \times 10^8$ yr (Rees 1984). The Eddington time t_E describes the time necessary to radiate at the Eddington luminosity the entire rest mass of an object. In hierarchical models for structure formation the first baryonic objects which collapsed had masses of the order of $\sim 10^4 - 10^6 M_\odot$ (e.g., Silk & Rees 1998; Larson 2000; Shibata & Shapiro 2002; Bromm & Loeb 2003). This provides upper limit estimates for M_{bh}^{seed} of black holes. Recent models of early star formation indicate that nearly metal free Pop III stars, formed at high-redshifts ($z \gtrsim 20$), were predominantly very massive with $M \gtrsim 100 M_\odot$ (e.g., Fryer, Woosley, & Heger 2001; Abel, Bryan, & Norman 2002; Bromm, Coppi, & Larson 2002). The stellar remnants are expected to be of the order of $\sim 10 M_\odot$ (e.g., Fryer 1999). However, some early star formation models even indicate the possibility of black hole remnants with several times $\sim 10^3 M_\odot$ (Bond, Arnett, & Carr 1984). In the following the efficiency ϵ to convert mass to energy is assumed to be $\epsilon = 0.1$. It should be noted that the efficiency ϵ can reach values up to $\epsilon = 0.42$ for a maximal rotating Kerr black hole.

We employed equation (2) to derive the time τ which is necessary to accumulate the determined mean black hole mass (Table 3) for seed black holes with $M_{bh}^{seed} = 10 M_\odot$, $10^3 M_\odot$, and $10^5 M_\odot$, respectively. We find that the time τ to build-up a SMBH is between several 100 Myr and ~ 1 Gyr, i.e., almost always τ is smaller than the age of the universe at the corresponding redshift. To illustrate this in a proper way we used τ to calculate t_o , i.e. the epoch when the SMBH, observed at t_{obs} , started to form. In Figure 4 the time t_o is displayed as a function of the observed redshift z_{obs} . The determined time scales τ and hence t_o indicate that most of the SMBH residing in the observed high-redshift quasars started to grow at redshifts of $z(t_o) \simeq 5$ to 10. As can be seen for low massive black hole seeds, i.e., stellar

remnants with $M_{bh}^{seed} \simeq 10M_{\odot}$ some black holes had to have started to grow at very early epochs and for Q 0105–2634 and SDSS 0388+0021 the required time τ is even larger than the actual cosmic age at z_{obs} . To avoid too long growing times τ , higher M_{bh}^{seed} masses appear to be favored. Assuming high mass seed black holes with $M_{bh}^{seed} = 10^3$ to 10^5M_{\odot} , the SMBH in the $z \simeq 3.5$ quasars began to grow at redshifts $z(t_o) \simeq 4$ and earlier. The luminous quasars at redshifts $z \gtrsim 4.5$ show a smaller scatter for t_o compared to those at $z \simeq 3.5$. Based on our results the SMBH residing in the $z \gtrsim 4.5$ quasars started at $z(t_o) \simeq 5$ to 10. However, stellar mass black hole seed are still a valid option because a flatter slope of the R – L relation for H β with $\beta \simeq 0.6$ (Peterson et al. 2000; McLure & Jarvis 2002) will yield about two times less massive black holes. Hence, the Eddington luminosity will be reduced and the Eddington ratio will be increased. As a result the growing time scale τ will decrease and SMBHs can be built-up with stellar mass remnants as black hole seeds as well.

It is remarkable that most of the super-massive black holes of the studied high-redshift quasars are in place at the end of the era of reionization of the universe which is supposed to end at $z \simeq 6$ (e.g., Becker et al. 2001; Fan et al. 2002). Particularly, for the quasars at redshifts $z \gtrsim 4.5$ we want to emphasize that the epoch when these black holes started to grow coincides with the beginning of first intense star formation that marks early phases of the host galaxy formation. This epoch of major star formation also is indicated by the chemical enrichment history of the quasar gas. To achieve the estimated metallicities of several times solar (e.g., Dietrich et al. 2003b,c) a major and intense star formation episode had to start at $z \simeq 6$ to 8. Further circumstantial evidence for a vigorous star formation phase at those high-redshifts is given by the lack of evolution of the iron/ α element ratio compared to results for local quasars (e.g., Barth et al. 2003; Dietrich et al. 2002, 2003a; Freudling et al. 2003; Iwamuro et al. 2002; Maiolino et al. 2003; Thompson et al. 1999).

The presence of super-massive black holes in luminous high-redshift quasars, the estimated time scale required to build-up black holes of several $M_{bh} \simeq 10^9M_{\odot}$, the gas metallicity of at least solar up to several times solar, and the lack of evolution of the relative iron/ α element abundance ratio provide evidence that those quasars reside in already mature host galaxies, at least with an evolved massive central component (Hamann et al. 2004). While the massive galaxy is forming, i.e., major and vigorous star formation activity occurs, the super-massive black hole grows. It takes about ~ 0.5 Gyr to accumulate a SMBH with several times $M_{bh} \simeq 10^8M_{\odot}$ to $M_{bh} \simeq 10^9M_{\odot}$ that is necessary to power quasar activity. It takes approximately this same amount of time for a stellar population to enrich the gas around quasars to the observed solar or super-solar levels (e.g., Dietrich et al. 2003b,c; Matteucci & Padovani 1993; Matteucci & Recchi 2001). Therefore, by the time most quasars become visible, even at the highest redshifts, a substantially evolved stellar population is harboring the active nucleus. This conclusion is supported by some theoretical models of

joint SMBH – host galaxy evolution (Archibald et al. 2002, Kawakatu et al. 2003). Direct imaging studies of low redshift quasars show clearly that the host galaxies are characterized by at least moderately old, stellar populations on $>\text{kpc}$ scale (Nolan et al. 2001; Dunlop et al. 2003). Although there is less imaging data at higher redshifts at least some quasars still have substantial hosts (Kukula et al. 2001).

It can be assumed that early phases of galaxy formation that are accompanied by intense and vigorous star formation also mark the era when super-massive black holes are growing from massive seed remnants (Hamann et al. 2004). A joint era of SMBH growth and early phases of galaxy formation can be understood in the context of recently suggested galaxy formation models (e.g., Archibald et al. 2002; Di Matteo et al. 2003; Granato et al. 2001, 2004). These models further suggest that the $M_{bh} \propto \sigma_*^4$ relation evolves over cosmic time scales and is finally established in the local universe (Di Matteo et al. 2003). A less steep $M_{bh} \propto \sigma_*$ relation also has been suggested by Shields et al. (2003). This may provide an explanation to avoid huge host galaxy masses ($\sim 10^{13} M_\odot$) and large stellar velocity dispersions ($\sigma_* \simeq 700 \text{ km s}^{-1}$) which have never been observed (e.g., Netzer 2003).

6. Conclusion

We have analyzed a sample of 15 luminous high-redshift quasars ($3.3 \lesssim z \lesssim 5.1$) to estimate the mass of super-massive black holes. For the first time results for M_{bh} based on three different emission lines, C IV, Mg II, and H β , are compared for high-redshift quasars.

We determine black hole masses in the range of $M_{bh} \simeq 2 \times 10^8 M_\odot$ up to $M_{bh} \simeq 4 \times 10^{10} M_\odot$. Similar to prior studies there appears to be an approximate upper limit for M_{bh} at $\sim 10^{10} M_\odot$. The black hole mass estimates based on C IV and H β are quite consistent while Mg II indicates by a factor of ~ 5 lower SMBH masses. In spite of the uncertainties regarding the use of the H β , Mg II, and C IV emission line profiles to determine the black hole mass, all three emission lines indicate consistently the presence of super-massive black holes with masses on average $\sim 6 \times 10^9 M_\odot$ at redshifts up to $z=5.1$.

We determine an Eddington luminosity ratio of L_{bol}/L_{edd} in the range of ~ 0.5 to ~ 7 . This is consistent with results of studies of quasars sample that are dominated by low and intermediate redshift quasars. This indicates that high-redshift quasars are not different regarding the Eddington ratio L_{bol}/L_{edd} compared to those at lower redshift.

To date the epoch when the SMBHs which drive high-redshift quasar activity should have started to grow, we assume logarithmic growth by spherical accretion with a mass to energy conversion efficiency of $\epsilon = 0.1$. Generally, the growth-time τ is of the order of several

~ 100 Myr Assuming higher mass seed black holes ($M_{bh}^{seed} = 10^3$ to $10^5 M_{\odot}$) the SMBH in the $z \simeq 3.5$ quasars begun to grow at redshifts $z(t_o) \simeq 4$ and earlier while the quasars with $z \gtrsim 4.5$ started at $z(t_o) \simeq 5$ to 10.

The presence of super-massive black holes in luminous high-redshift quasars, the estimated time scale required to build-up black holes of several times $M_{bh} \simeq 10^9 M_{\odot}$, the several times solar gas metallicity and the lack of evolution of the relative iron/ α element abundance ratio provide evidence that luminous quasars at high-redshift reside in already mature host galaxies, at least with an substantially evolved massive central stellar component. This result indicates that early phases of massive galaxy formation that are accompanied by intense and vigorous star formation also mark the era when super-massive black holes are growing from massive seed remnants. The estimated black hole growth time scale suggest a delay of about ~ 0.5 Gyr of the quasar activity with respect to preceding intense star formation which is consistent with the observed high gas metallicity.

We dedicate this Paper to the memory of Richard J. Elston, who left us far too early on January 26, 2004.

MD and FH acknowledge support from NASA grant NAG 5-3234 and NSF grant AST-99-84040 (University of Florida).

A. Appendix

The equations we applied, given by Kaspi et al. (2000), McLure & Jarvis (2002), Vestergaard (2002), and Warner et al. (2003) have been modified for the use of the continuum luminosity L_{λ} that we measured at $\lambda = 1450 \text{ \AA}$ for each of the high-redshift quasars of this study. We explicitly present the dependence on the spectral index α which transforms the continuum luminosity measured at different wavelengths. The uniform use of $L_{\lambda}(1450 \text{ \AA})$ does not introduce an additional uncertainty, because instead of assuming a fixed continuum slope α to rescale L_{λ} as in prior studies we used the measured continuum slope α for each quasar which we determined for the power-law continuum fit ($F_{\nu} \propto \nu^{\alpha}$, Table 2) in the multi-component analysis of the quasar spectra (Dietrich et al. 2002a, 2003a). The continuum slope is measured for a wavelength range of $\lambda \lambda \sim 1100$ to 5500 \AA ($z = 3.5$ quasars) and $\lambda \lambda \sim 1100$ to 4300 \AA ($z = 4.5$ quasars).

For the H β emission line profile we determined M_{bh} applying the equation given by Kaspi et al. (2000) (eq. A1) and presented by McLure & Jarvis (2002) (eq. A2). The main difference is given by the slope of the radius – luminosity (R – L) relation.

$$M_{bh} = 4.82 \times 10^6 \times \left(\frac{1450}{5100} \right)^{0.7(1+\alpha)} \times \left(\frac{\lambda L_\lambda(1450\text{\AA})}{10^{44} \text{ erg/s}} \right)^{0.7} \times \left(\frac{\text{FWHM}(H\beta)}{10^3 \text{ km/s}} \right)^2 M_\odot \quad (\text{A1})$$

$$M_{bh} = 4.74 \times 10^6 \times \left(\frac{1450}{5100} \right)^{0.61(1+\alpha)} \times \left(\frac{\lambda L_\lambda(1450\text{\AA})}{10^{44} \text{ erg/s}} \right)^{0.61} \times \left(\frac{\text{FWHM}(H\beta)}{10^3 \text{ km/s}} \right)^2 M_\odot \quad (\text{A2})$$

The black hole mass is estimated based on the CIV λ 1549 line profile width applying the following equations (Vestergaard 2002, eq. A3; Warner et al. 2003, eq. A4). Warner et al. (2003) assumed that the radius of the CIV BLR is half the size of the H β emitting region which is well justified by variability studies (Peterson 1993).

$$M_{bh} = 1.58 \times 10^6 \times \left(\frac{1450}{1350} \right)^{0.7(1+\alpha)} \times \left(\frac{\lambda L_\lambda(1450\text{\AA})}{10^{44} \text{ erg/s}} \right)^{0.7} \times \left(\frac{\text{FWHM}(\text{CIV})}{10^3 \text{ km/s}} \right)^2 M_\odot \quad (\text{A3})$$

$$M_{bh} = 2.41 \times 10^6 \times \left(\frac{1450}{5100} \right)^{0.7(1+\alpha)} \times \left(\frac{\lambda L_\lambda(1450\text{\AA})}{10^{44} \text{ erg/s}} \right)^{0.7} \times \left(\frac{\text{FWHM}(\text{CIV})}{10^3 \text{ km/s}} \right)^2 M_\odot \quad (\text{A4})$$

To estimate M_{bh} based on the Mg II λ 2798 emission line profile width we employed the relation given by McLure & Jarvis (2002).

$$M_{bh} = 3.37 \times 10^6 \times \left(\frac{1450}{3000} \right)^{0.47(1+\alpha)} \times \left(\frac{\lambda L_\lambda(1450\text{\AA})}{10^{44} \text{ erg/s}} \right)^{0.47} \times \left(\frac{\text{FWHM}(\text{MgII})}{10^3 \text{ km/s}} \right)^2 M_\odot \quad (\text{A5})$$

REFERENCES

Abel, T., Bryan, G.L., & Norman, M.L. 2002, Science, 295, 93

Archibald, E.N., Dunlop, J.S., Jimenez, R., Fria\c{c}a, A.C.S., McLure, R.J., & Hughes, D.H. 2002, MNRAS, 336, 353

Barth, A.J. 2003, in "Coevolution of Black Holes and Galaxies", Carnegie Observatories Astrophysics Series, Vol.I, ed. L.C. Ho (Cambridge: Cambridge Univ. Press), in press

Barth, A.J., Martini, P., Nelson, C.H., Ho, L.C. 2003, ApJ, 594, L95

Bechthold, J., Siemiginowska, A., Shields, J., et al. 2003, *ApJ*, 588, 119

Becker, R.H., et al. 2001, *AJ*, 122, 2850

Bond, J.R., Arnett, W.D., & Carr, B.J. 1984, *ApJ*, 280, 825

Boroson, T.A. & Green, R.F. 1992, *ApJS*, 80, 109

Bromm, V., Coppi, P.S., & Larson, R.B. 2002, *ApJ*, 564, 23

Bromm, V. & Loeb, A. 2003, *ApJ*, 596, 34

Bromm, V., Yoshida, N., & Hernquist, L. 2003, *ApJ*, 596, L1

Cattaneo, A., Haehnelt, M.G., & Rees, M.J. 1999, *MNRAS*, 308, 77

Clavel, J., Reichert, G.A., Alloin, D., et al. 1991, *ApJ*, 366, 64

Corbett, E.A., Croom, S.M., Boyle, B.J., et al. 2003, *MNRAS*, 343, 705

Dietrich, M., Appenzeller, I., Wagner, S.J., et al. 1999, *A&A*, 352, L1

Dietrich, M., Appenzeller, I., Vestergaard, M., & Wagner, S.J. 2002a, *ApJ*, 564, 581

Dietrich, M., Hamann, F., Shields, J.C., et al. 2002b, *ApJ*, 581, 912

Dietrich, M., Hamann, F., Appenzeller, I., & Vestergaard, M. 2003a, *ApJ*, 596, 817

Dietrich, M., Appenzeller, I., Hamann, F., Heidt, J., Jäger, K., Vestergaard, M., & Wagner, S.J. 2003b, *A&A*, 398, 891

Dietrich, M., Hamann, F., Shields, J.C., Constantin, A., Heidt, J., Jäger, K., Vestergaard, M., & Wagner, S.J. 2003c, *ApJ*, 589, 722

Dietrich, M. & Kollatschny, W. 1995, *A&A*, 303, 405

Dietrich, M. & Wilhelm-Erkens, U. 2000, *A&A*, 354, 17

Di Matteo, T., Croft, R.A.C., Springel, V., & Hernquist, L. 2003, *ApJ*, 593, 56

Dunlop, J.S., McLure, R.J., Kukula, M.J., Baum, S.A., O'Dea, C.P., & Hughes, D.H. 2003, *MNRAS*, 340, 1095

Elvis, M., Wilkes, B.J., McDowell, J.C., et al. 1994, *ApJS*, 95, 1

Fan, X., Narayanan, V.K., Lupton, R.H., et al. 2001, *AJ*, 122, 2833

Ferrarese, L., Pogge, R.W., Peterson, B.M., Merritt, D., Wandel, A., & Joseph, C.L. 2001, ApJ, 555, L79

Freudling, W., Corbin, M.R., & Korista, K.T. 2003, ApJ, 587, L67

Fryer, C.L. 1999, ApJ, 522, 413

Fryer, C.L., Woosley, S.E., & Heger, A. 2001, ApJ, 550, 372

Gebhardt, K., et al. 2000, ApJ, 543, L5

Graham, A.W., Erwin, P., Caon, N., & Trujillo, I. 2001, ApJ, 563, L11

Granato, G.L., Silva, L., Monaco, P., Panuzzo, P., Salucci, P., DeZotti, G., & Danese, L. 2001, MNRAS, 324, 757

Granato, G.L., DeZotti, G., Silva, L., Bressan, A., & Danese, L. 2004, ApJ, 600, 580

Grandi, S.A. 1982, ApJ, 255, 25

Haiman, Z. & Loeb, A. 2001, ApJ, 552, 459

Hamann, F., Dietrich, M., Sabra, B., & Warner C. 2004, in "Origin and Evolution of the Elements", Carnegie Observatories Astrophysics Series, Vol.IV, ed. A. McWilliams and M. Rauch (Cambridge: Cambridge Univ. Press), in press

Iwamuro, F., et al. 2002, ApJ, 565, 63

Kaspi, S., Smith, P.S., Netzer, H., Maoz, D., Jannuzi, B.T., & Giveon, U. 2000, ApJ, 533, 631

Kauffmann, G. & Haehnelt, M.G. 2000, MNRAS, 311, 576

Kawakatu, N., Umemura, M., & Mori, M. 2003, ApJ, 583, 85

Kormendy, J. & Richstone, D. 1995, ARA&A, 33, 581

Krolik, J.H. 2001, ApJ, 551, 72

Kukula, M.J., Dunlop, J.S., McLure, R.J., et al. 2001, MNRAS, 326, 1533

Laor, A. 2001, ApJ, 553, 677

Larson, R.B. 2000, in Proc. 33d ESLAB Symp., Star Formation from the Small to the Large Scale, ed. F. Favata, A.A. Klaas, & A. Wilson (ESA SP-445; Noordwijk:ESA), (preprint astro-ph/9912539)

Magorrian, J., Tremaine, S., & Richstone, D. 1998, AJ, 115, 2285

Maiolino, R., Juarez, Y., Mujica, R., Nagar, N.M., & Oliva, E. 2003, ApJ, 596, L155

Matteucci, F. & Padovani, P. 1993, ApJ, 419, 485

Matteucci, F. & Recchi, S. 2001, ApJ, 558, 351

McLure, R.J., Dunlop, J.S., Kukula, M.J., Baum, S.A., O'Dea, C.P., & Hughes, D.H. 1999, MNRAS, 308, 377

McLure, R.J. & Dunlop, J.S. 2001, MNRAS, 327, 199

McLure, R.J. & Dunlop, J.S. 2002, MNRAS, 331, 795

McLure, R.J. & Jarvis, M.J. 2002, MNRAS, 337, 109

Menou, K., Haiman, Z., & Narayanan, V.K. 2001, ApJ, 558, 535

Merritt, D. & Ferrarese, L. 2000, ApJ,

Merritt, D. & Ferrarese, L. 2001, ApJ, 547, 140

Nelson, C.H. 2000, ApJ, 544, L91

Netterfield, C.B., et al. 2002, ApJ, 571, 604

Netzer, H. 2003, ApJ, 583, L5

Nolan, L.A., Dunlop, J.S., Kukula, M.J., Hughes, D.H., Boroson, T., & Jimenez, R. 2001, MNRAS, 323, 308

Onken, C.A. & Peterson, B.M. 2002, ApJ, 572, 746

Percival, W.J., Miller, L., McLure, R.J., & Dunlop, J.S. 2001, MNRAS, 322, 843

Peterson, B.M. 1993, PASP, 105, 247

Peterson, B.M. 1997, in ‘An Introduction to active galactic nuclei’, Cambridge University Press

Peterson, B.M., Balonek, T.J., Barker, E.S., et al. 1991, ApJ, 368, 119

Peterson, B.M. & Wandel, A. 1999, ApJ, 521, L95

Peterson, B.M. & Wandel, A. 2000, ApJ, 540, L13

Peterson, B.M., McHardy, I.M., Wilkes, B.J., et al. 2000, *ApJ*, 542, 161

Rees, M.J. 1984, *ARA&A*, 22, 471

Reichert, G.A., Rodriguez-Pascual, P.M., Alloin, D., et al. 1994, *ApJ*, 425, 582

Rocca-Volmerange, B., LeBorgne, D., DeBeuck, C., Fioc, M., & Moy, E. 2004, *A&A*, 415, 931

Salucci, P., Szuszkiewicz, E., Monaco, P., & Danese, L. 1999, *MNRAS*, 307, 637

Shibata, M. & Shapiro, S.L. 2002, *ApJ*, 572, L39

Silk, J. & Rees, M.J. 1998, *A&A*, 331, L1

Shields, G.A., Gebhardt, K., Salviander, S., et al. 2003, *ApJ*, 583, 124

Stirpe, G.M., Winge, C., Altieri, B., et al. 1994, *ApJ*, 425, 609

Storey, P.J. & Hummer, D.G. 1995, *MNRAS*, 272, 41

Thompson, K.L., Hill, G.J., & Elston, R. 1999, *ApJ*, 515, 487

Tremaine, S., et al. 2002, *ApJ*, 574, 740

Umemura, M., in "Coevolution of Black Holes and Galaxies", Carnegie Observatories Astrophysics Series, Vol.I, ed. L.C. Ho

Vestergaard, M. & Wilkes, B.J. 2001, *ApJS*, 134, 1

Vestergaard, M. 2002, *ApJ*, 571, 733

Vestergaard, M. 2004, *ApJ*, 601, 676

Wandel, A., Peterson, B.M., & Malkan, M.A. 1999, *ApJ*, 526, 579

Warner, C., Hamann, F., & Dietrich, M. 2003, *ApJ*, 596, 72

Warner, C., Hamann, F., & Dietrich, M. 2004, *ApJ*, in press

Willott, C.J., McLure, R.J., & Jarvis, M.J. 2003, *ApJ*, 587, L15

Wills B.J., Netzer, H., & Wills, D. 1985, *ApJ*, 288, 94

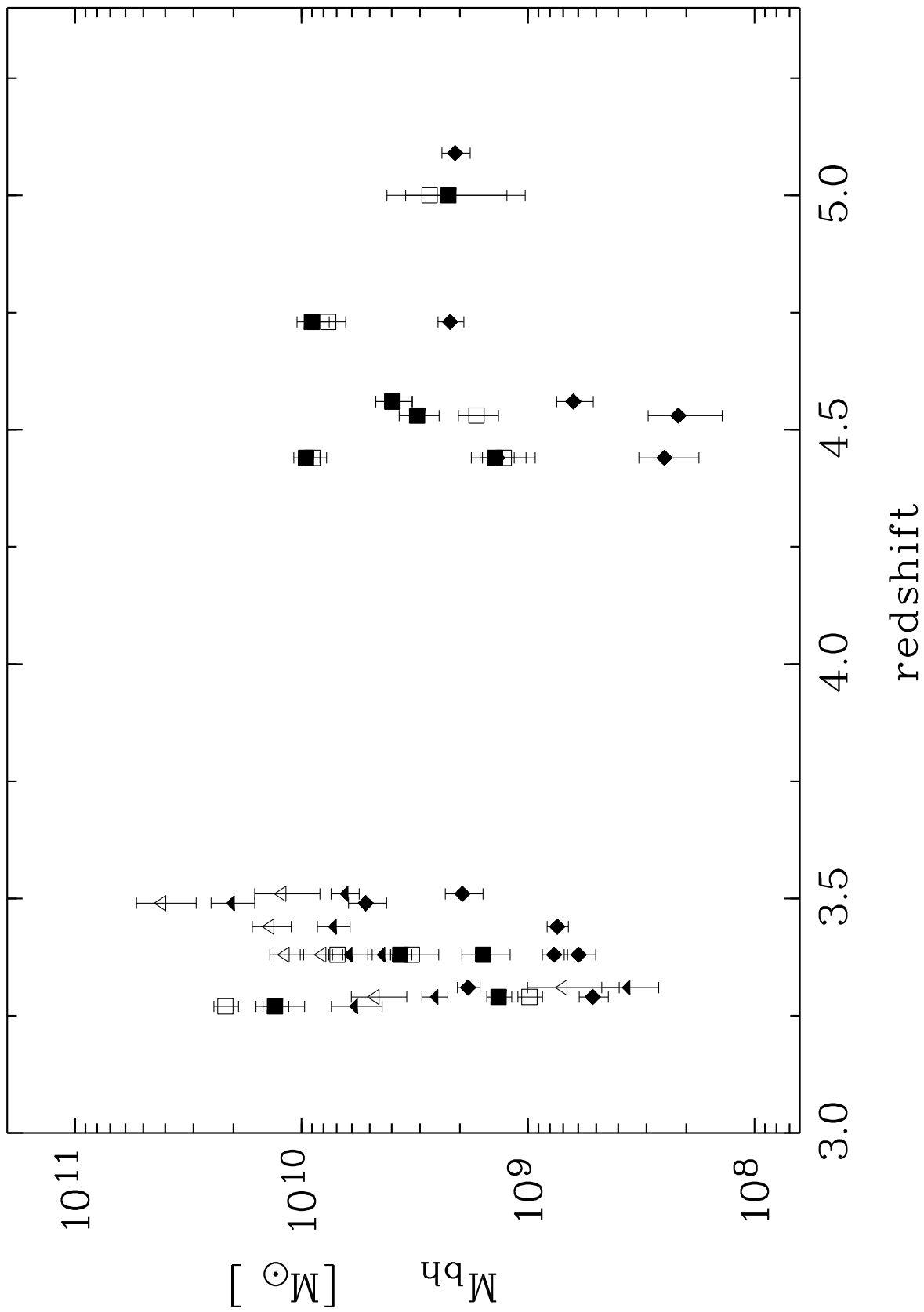
Woo, J.-H. & Urry, C.M. 2002, *ApJ*, 579, 530

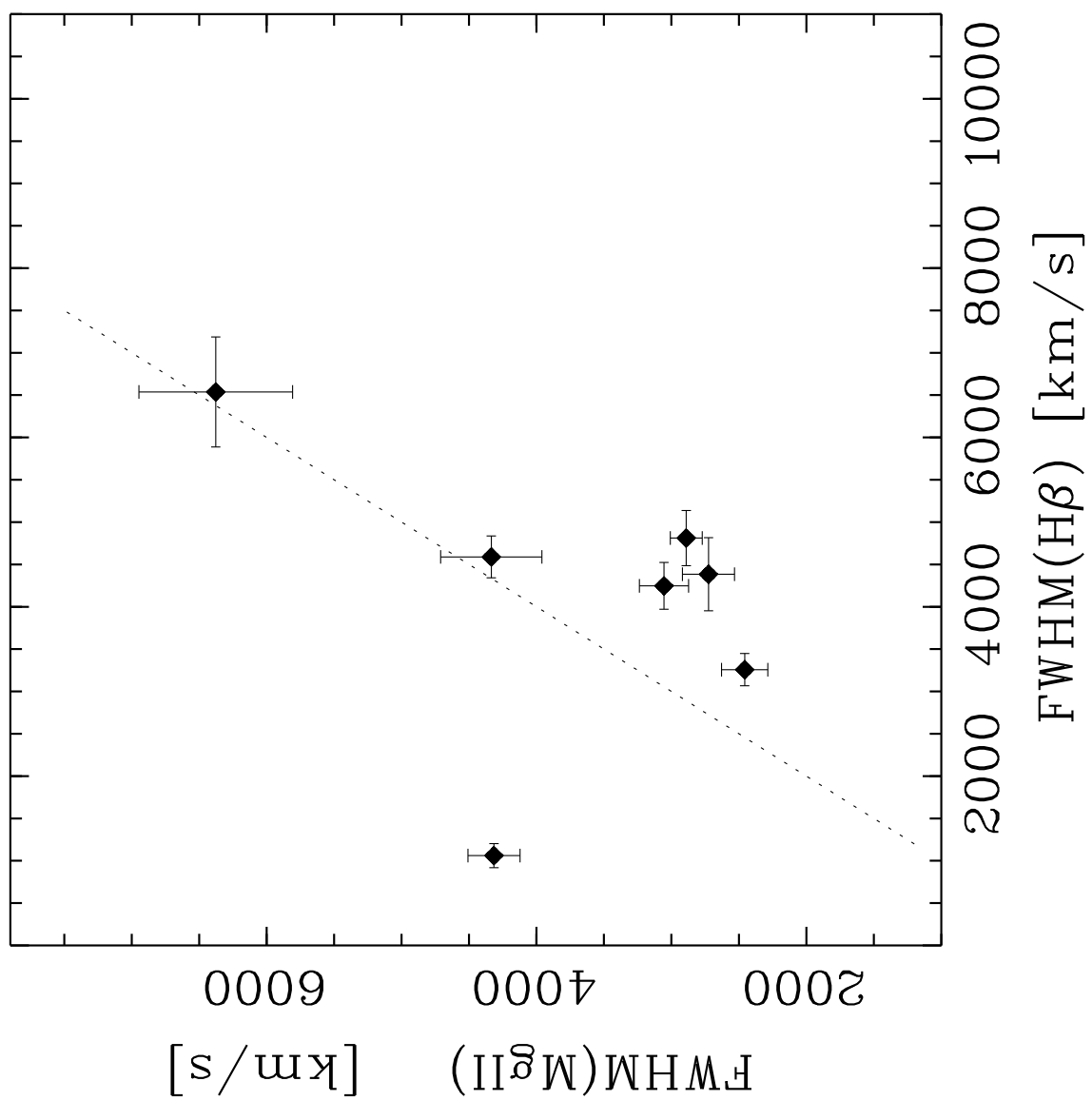
Fig. 1.— Estimates SMBH masses for the high-redshift quasars as a function of redshift using eq. (A1) to (A5). The triangles indicate M_{bh} based on H β (\triangle – Kaspi et al. 2000; \blacktriangle – McLure & Jarvis 2002), the squared symbols show M_{bh} based on C IV (\square – Warner et al. 2003; \blacksquare – Vestergaard 2002), and the filled diamonds display M_{bh} based on Mg II (\blacklozenge – McLure & Jarvis 2002).

Fig. 2.— Comparison of the line profile width, FWHM, of Mg II $\lambda 2798$ and H β for the high-redshift quasars at $z \simeq 3.5$. The dotted line indicates a perfect one-to-one relation.

Fig. 3.— Mean SMBH masses for the high-redshift quasars as a function of bolometric luminosity, L_{bol} , are shown. The displayed errors are taking into account the measurement uncertainties and the distribution of the individual SMBH mass estimates in quadrature (Table 3).

Fig. 4.— The time $t_o = \tau_{obs} - \tau$ is plotted as a function of redshift for several seed black hole masses to illustrate when the super-massive black holes had to start to form. The three panels display results for different seed black hole masses with $M_{bh}^{seed} = 10M_\odot$ (left), $M_{bh}^{seed} = 10^3M_\odot$ (center), and $M_{bh}^{seed} = 10^5M_\odot$ (right). The redshift which corresponds to t_o is labeled at the right as $z(t_o)$ ($H_o = 65 \text{ km s}^{-1} \text{ Mpc}^{-1}$, $\Omega_M = 0.3$, $\Omega_\Lambda = 0.0$).





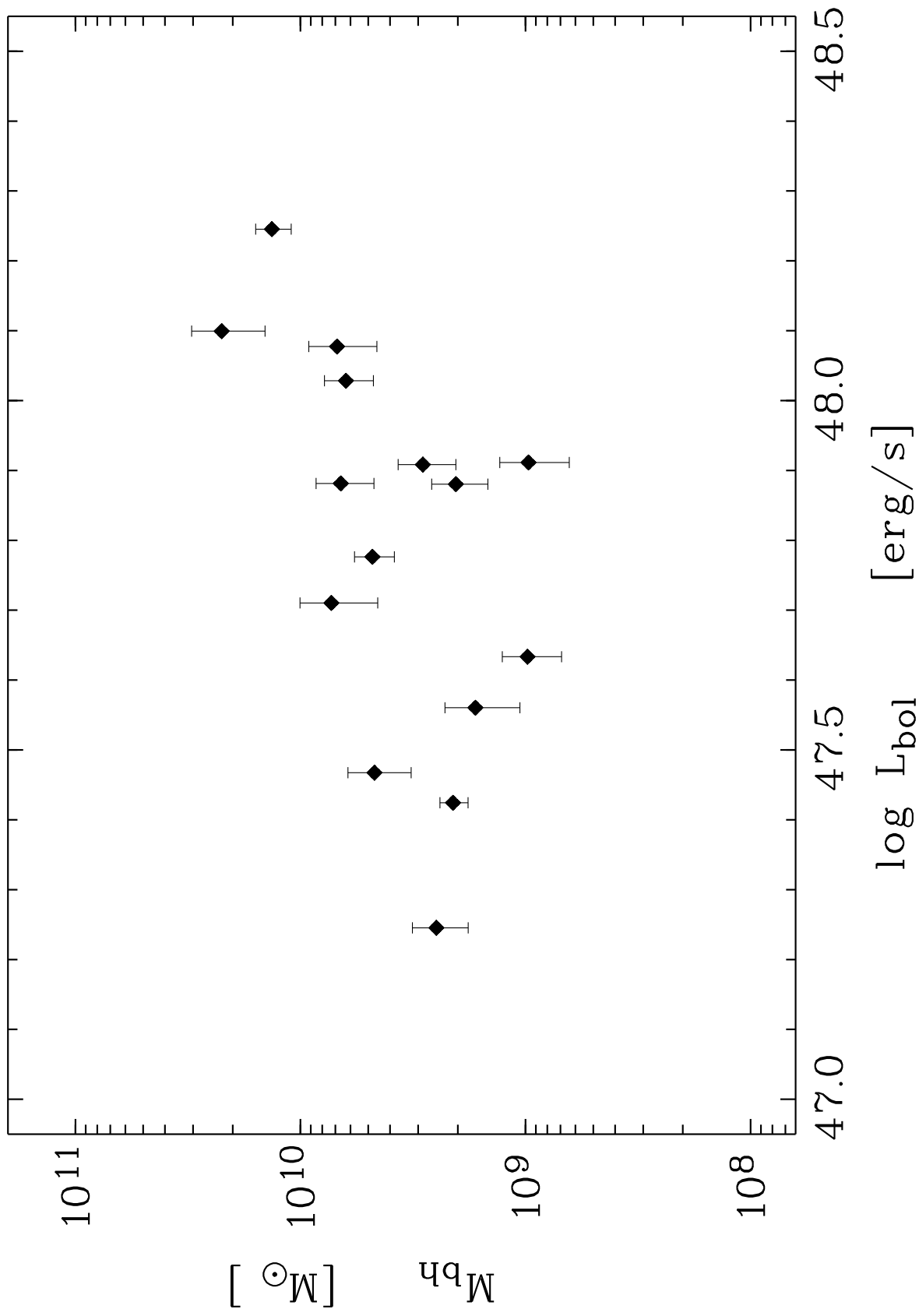


Table 1. The high-redshift quasars have been observed at the observatories and dates as given in (2) and (3). In addition, the achieved spectral resolution for the emission line profiles of H β , Mg II, and C IV is listed in unit of km s $^{-1}$ (columns 4 to 6). The redshift of the quasars is given in (7). The rest frame continuum luminosity $\lambda L_\lambda(1450\text{\AA})$ and the bolometric luminosity, L_{bol} , are listed in (8) and (9).

quasar	site	date	CIV	resol. MgII [km s $^{-1}$]	H β	redshift (7)	log $\lambda L_\lambda(1450\text{\AA})$ [erg s $^{-1}$] (8)	log L_{bol} [erg s $^{-1}$] (9)
(1)	(2)	(3)	(4)	(5)	(6)			
BRI 0019-1522	CTIO	09-00	300	230	...	4.53	46.92	47.56
BR 0103+0032	CTIO	09-00	300	230	...	4.44	46.99	47.63
Q 0103-260	VLT	12-98	750	3.38	46.83	47.47
	NTT	10-99	...	500	430			
Q 0105-2634	NTT	10-99	...	500	430	3.49	47.46	48.10
PSS J0248+1802	CTIO	09-00	300	230	...	4.44	47.24	47.88
Q 0256-0000	NTT	10-99	300	500	430	3.38	47.14	47.78
Q 0302-0019	NTT	09-99	300	500	430	3.29	47.24	47.88
SDSS 0338+0021	VLT	12-98	750	5.00	46.61	47.25
PC 1158+4635	KECK	05-00	300	520	...	4.73	47.39	48.03
SDSS 1204-0021	VLT	04-01	...	525	...	5.09	46.79	47.42
Q 2050-259	CTIO	09-00	...	230	230	3.51	47.44	48.08
PKS 2126-158	CA	08-93	300	3.27	47.61	48.25
	CTIO	09-00	...	230	230			
Q 2227-3928	NTT	10-99	...	500	430	3.44	47.07	47.71
BRI 2237-0607	CTIO	09-00	300	230	...	4.56	47.27	47.91
Q 2348-4025	NTT	10-99	...	500	430	3.31	47.27	47.91

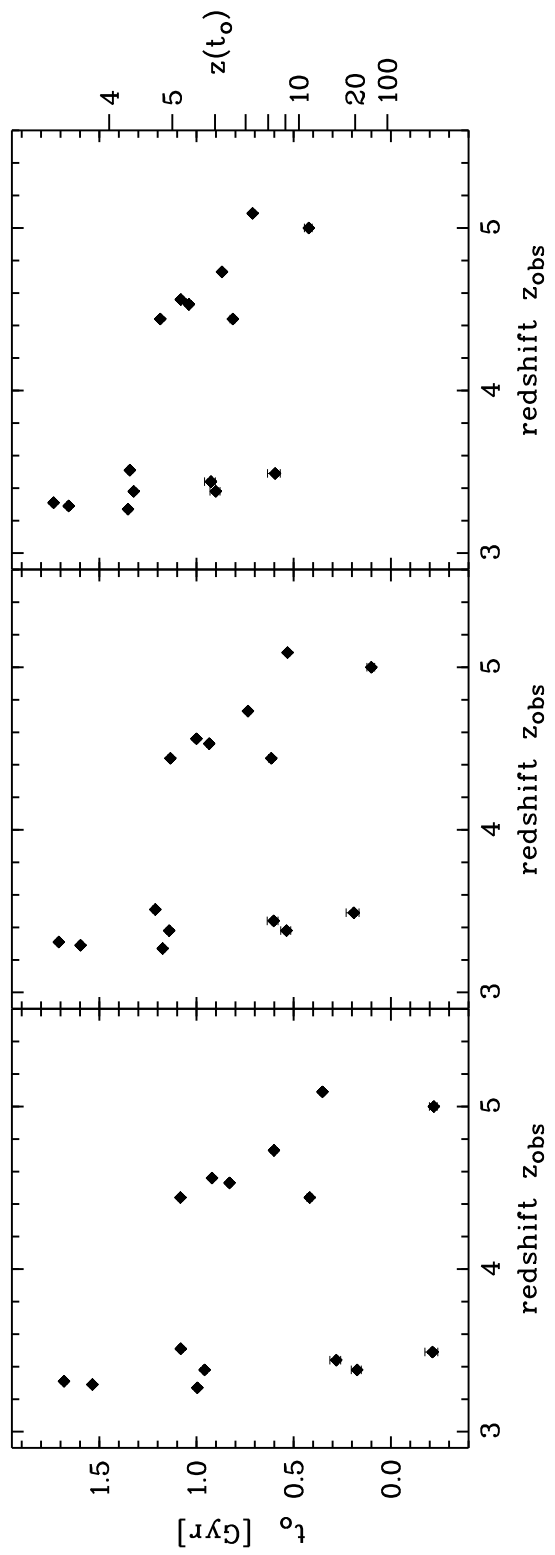


Table 2. Measurements of the emission line profile widths (FWHM) for H β , Mg II $\lambda 2798$, and C IV $\lambda 1549$ are given for the studied high-redshift quasar sample. The slope α of the power-law continuum fit ($F_\nu \propto \nu^\alpha$) given in column (5).

quasar	FWHM(H β)	FWHM(Mg II) [km s $^{-1}$]	FWHM(C IV)	α
(1)	(2)	(3)	(4)	(5)
BRI 0019-1522	...	1993 \pm 353	4078 \pm 347	+0.10 \pm 0.09
BR 0103+0032	...	1869 \pm 268	2626 \pm 118	-0.46 \pm 0.03
Q 0103-260	4384 \pm 432	2725 \pm 193	3257 \pm 350	-1.33 \pm 0.06
Q 0105-2634	6537 \pm 650	6377 \pm 570	...	-0.69 \pm 0.06
PSS J0248+1802	...	3811 \pm 279	5620 \pm 224	-0.48 \pm 0.08
Q 0256-0000	4247 \pm 277	3055 \pm 182	3784 \pm 163	-0.41 \pm 0.05
Q 0302-0019	3257 \pm 191	2457 \pm 171	2102 \pm 108	-0.21 \pm 0.03
SDSS 0338+0021	4500 \pm 1200	-0.01 \pm 0.20
PC 1158+4635	...	4559 \pm 257	4833 \pm 300	-0.37 \pm 0.05
SDSS 1204-0021	...	6090 \pm 380	...	-0.43 \pm 0.06
Q 2050-259	4589 \pm 247	4335 \pm 375	...	-0.15 \pm 0.18
PKS 2126-158	2707 \pm 320	...	4991 \pm 176	-1.09 \pm 0.09
Q 2227-3928	4812 \pm 326	2890 \pm 118	...	-0.85 \pm 0.05
BRI 2237-0607	...	2517 \pm 214	3550 \pm 269	-0.55 \pm 0.02
Q 2348-4025	1061 \pm 142	4315 \pm 193	...	-0.53 \pm 0.07

Table 3. The SMBH masses estimates for the studied high-redshift quasar sample. The derived black hole masses based on $H\beta$ using Kaspi et al. (2000, K00) and McLure & Jarvis (2002, MJ02) are given in (2) and (3). The SMBH estimates employing $C\text{IV}\lambda 1549$ are listed in column (4) and (5) (Vestergaard 2002, MV02; Warner et al 2003, CW03) and using $Mg\text{II}\lambda 2798$ in (6) (McLure & Jarvis 2002, MJ02). In column (7) the mean super-massive black hole mass is listed and the resulting Eddington ratio L_{bol}/L_{edd} is given in column (8).

quasar	$H\beta$ (K00)	$H\beta$ (MJ02)	$C\text{IV}$ (MV02) $M_{bh} [10^9 M_\odot]$	$C\text{IV}$ (CW03)	$Mg\text{II}$ (MJ02)	M_{bh} $[10^9 M_\odot]$	L_{bol}/L_{edd}
(1)	(2)	(3)	(4)	(5)	(6)	(7)	(8)
BRI 0019-1522	3.1 ± 0.6	1.7 ± 0.3	0.22 ± 0.08	1.7 ± 0.6	1.73
BR 0103+0032	1.4 ± 0.4	1.3 ± 0.4	0.25 ± 0.07	1.0 ± 0.3	3.48
Q 0103-260	11.8 ± 2.0	6.2 ± 1.3	1.6 ± 0.4	3.3 ± 0.8	0.60 ± 0.10	4.7 ± 1.5	0.50
Q 0105-2634	41.4 ± 12.2	20.6 ± 4.5	5.2 ± 1.0	22.4 ± 8.0	0.45
PSS J0248+1802	9.6 ± 1.3	8.9 ± 1.2	1.4 ± 0.2	6.6 ± 1.9	0.91
Q 0256-0000	8.1 ± 2.0	4.5 ± 0.6	3.7 ± 1.4	6.9 ± 0.4	0.77 ± 0.10	4.8 ± 0.9	0.99
Q 0302-0019	4.7 ± 1.3	2.6 ± 0.3	1.4 ± 0.2	1.0 ± 0.1	0.52 ± 0.08	2.0 ± 0.6	2.95
SDSS 0338+0021	2.3 ± 1.2	2.7 ± 1.5	...	2.5 ± 0.7	0.56
PC 1158+4635	9.0 ± 1.5	7.6 ± 1.2	2.2 ± 0.3	6.3 ± 1.5	1.35
SDSS 1204-0021	2.1 ± 0.3	2.1 ± 0.3	1.00
Q 2050-259	12.2 ± 3.9	6.5 ± 0.9	2.0 ± 0.4	6.9 ± 2.3	1.38
PKS 2126-158	12.8 ± 3.1	5.9 ± 1.5	13.1 ± 1.7	21.7 ± 2.7	...	13.4 ± 2.4	1.01
Q 2227-3928	13.8 ± 2.7	7.3 ± 1.2	0.74 ± 0.08	7.3 ± 1.5	0.56
BRI 2237-0607	4.0 ± 0.7	4.0 ± 0.7	0.63 ± 0.12	2.9 ± 0.8	2.25
Q 2348-4025	0.70 ± 0.30	0.37 ± 0.10	1.8 ± 0.2	1.0 ± 0.3	6.67